

NUMERICAL SIMULATION FOR FAST PYROLYSIS OF WOODY BIOMASS IN A BUBBLING FLUIDISED BED REACTOR

Hang Seok CHOI¹, Yeon Seok CHOI¹ and Seock Joon KIM¹

¹ Korea Institute of Machinery and Materials, 104 Sinseongno, Yuseong-gu, Daejeon, 305-343, South KOREA

ABSTRACT

In the present study, to investigate the fast pyrolysis characteristics of woody biomass in bubbling fluidised bed reactor, numerical approach is applied by using CFD (computational fluid dynamics). For the multiphase reacting flow fields between solid and gas, Eulerian-Eulerian approach is applied including three gas species and three solid phases. For the woody biomass pyrolysis, two-stage, semi-global reaction kinetics is adopted considering the secondary tar cracking mechanism. The flow and reaction characteristics of the reactor are fully investigated and in particular the rising bubble motion and its role for pyrolysis reaction are studied. Also, the region is analysed, where the secondary tar cracking reaction occurs for future work to increase oil yield by suppressing the secondary reaction. From the predicted results, it is fully scrutinized that the heat transfer between bed material and biomass is mainly governed by particular bubble motions and this influences the pyrolysis reaction.

Keywords: Biomass, CFD, Fast pyrolysis, Fluidised bed.

NOMENCLATURE

C_p	specific heat capacity at constant pressure, erg/g·K
D	diffusion coefficient for chemical species, g/m·s
F	coefficient for interphase force, g/cm ³ ·s
g	gravitational acceleration, cm ² /s
p	pressure, dyn/cm ²
T	temperature, K
t	time, s
q	conductive heat flux, erg/cm ² ·s
R	rate of production of chemical species, g/cm ³ ·s
RM	rate of mass transfer between phases, g/cm ³ ·s
S	solid phase stress tensor, dyn/cm ²
v	velocity, cm/s
Y	mass fraction of chemical species
ε	volume fraction
ρ	density, g/cm ³
τ_g	deviatoric stress tensor for gas phase, dyn/cm ²
γ	gas-solid heat transfer coefficient, erg/cm ³ ·K ⁴ ·s

INTRODUCTION

To overcome environmental and natural resource exhaustion problems caused by fossil fuels, biomass is one of the promising renewable energy sources and thermal treatment of biomass to energy has been widely applied in many countries (Brammer et al. 2006, Dong et al. 2006, Wu et al. 2009, Dahl et al. 2009). Especially, fast pyrolysis method becomes bright prospect for thermal

conversion of biomass into biocrude oil, which can be used for heat and power generation and additionally for bio-refinery (Brammer et al. 2006). For the fast pyrolysis, the bubbling fluidised bed reactor has been broadly used for lab-scale or pilot-scale plants because of its high heat transfer rate to biomass (Park et al. 2008, Zheng J. 2008, Velden et al. 2008). Until now, the numerical study for bubbling fluidised bed reactor has been intensively fulfilled in many industrial fields however there are a few numerical studies for fast pyrolysis by using bubbling fluidised bed reactor (Saastamoinen 2006, Papadikis et al. 2009a, Papadikis et al. 2009b). In the present study, to investigate the reacting flow fields of a bubbling fluidised bed reactor, computational fluid dynamics is applied by using MFIX code (Syamlal et al. 1993). For the multiphase reacting flow fields between solid and gas, Eulerian-Eulerian approach is applied for simplicity of the calculation including three gas species for volatile, non-condensable gas and N₂ and three solid phases for sand, wood and char. For the woody biomass pyrolysis, two-stage, semi-global reaction kinetics is adopted considering the secondary tar cracking mechanism. The flow and thermal characteristics of the reactor are fully investigated and in particular the rising bubble motion and its role for pyrolysis reaction are studied. Also, the region is analysed, where the secondary tar cracking reaction occurs for future work to increase oil yield by suppressing the secondary reaction. From the predicted results, it is fully scrutinized that the heat transfer between bed material and biomass is mainly governed by particular bubble motions and this influences the pyrolysis reaction. This computational work would be greatly helpful to design and scale-up biomass pyrolysis plant by fully predicting fast pyrolysis flow field of the reactor, which is hardly obtained from experiment.

MODEL DESCRIPTION

Governing Equations

The governing equations for gas-solid multiphase flow are chosen according to Wachem et al. (2001) and are given as follows.

For continuity equations

$$\frac{\partial}{\partial t}(\varepsilon_g \rho_g) + \nabla \cdot (\varepsilon_g \rho_g \mathbf{v}_g) = \sum_{\alpha=1}^n R_{\alpha} \quad (1)$$

$$\frac{\partial}{\partial t}(\varepsilon_{sj} \rho_{sj}) + \nabla \cdot (\varepsilon_{sj} \rho_{sj} \mathbf{v}_{sj}) = \sum_{\beta=1}^n R_{sj\beta} \quad (2)$$

here subscript 'g' and 'sj' mean gas and jth solid phase, respectively and ε is the volume fraction of gas or solid phase. The 'R' means rate of production of chemical species in gas or solid phase. The ' α ' and ' β ' represent α^{th}

and β^{th} chemical species in gas and solid phases, respectively.

For momentum equations

$$\frac{\partial}{\partial t}(\epsilon_g \rho_g \mathbf{v}_g) + \nabla \cdot (\epsilon_g \rho_g \mathbf{v}_g \mathbf{v}_g) = -\epsilon_g \nabla P_g + \nabla \cdot \boldsymbol{\tau}_g + \sum_{j=1}^n F_{gsj}(\mathbf{v}_{sj} - \mathbf{v}_g) + \epsilon_g \rho_g \mathbf{g} - \sum_{j=1}^n RM_{gsj}(\xi_{gsj} \mathbf{v}_{sj} + \xi'_{gsj} \mathbf{v}_g) \quad (3)$$

$$\frac{\partial}{\partial t}(\epsilon_{sj} \rho_{sj} \mathbf{v}_{sj}) + \nabla \cdot (\epsilon_{sj} \rho_{sj} \mathbf{v}_{sj} \mathbf{v}_{sj}) = -\epsilon_{sj} \nabla P_g + \nabla \cdot \mathbf{S}_{sj} - F_{gsj}(\mathbf{v}_{sj} - \mathbf{v}_g) + \sum_{k=1}^n F_{sksj}(\mathbf{v}_{sk} - \mathbf{v}_{sj}) + \epsilon_{sj} \rho_{sj} \mathbf{g} + RM_{gsj}(\xi_{gsj} \mathbf{v}_{sj} + \xi'_{gsj} \mathbf{v}_g) - \sum_{k=1}^n RM_{sksj}(\xi_{sjsk} \mathbf{v}_{sk} + \xi'_{sjsk} \mathbf{v}_{sj}) \quad (4)$$

here, \mathbf{v} is velocity vector and $\boldsymbol{\tau}_g$ and \mathbf{S}_{sj} are the gas phase deviatoric stress tensor and j^{th} solid phase stress tensor, respectively. The F_{gsj} and F_{sksj} are coefficient for interphase force between gas and solid phases and between solid phases, respectively. RM_{ml} is the rate of mass transfer from m^{th} phase to l^{th} phase. Factor ξ is defined as ξ_{ml} is equals to 1 if RM_{ml} is less than zero, otherwise $\xi_{ml} = 0$ and ξ'_{ml} is defined as $\xi'_{ml} = 1 - \xi_{ml}$.

For energy equations

$$\epsilon_g \rho_g C_{pg} \left(\frac{\partial T_g}{\partial t} + \mathbf{v}_g \cdot \nabla T_g \right) = -\nabla \cdot \mathbf{q}_g + \sum_{j=1}^n \gamma_{gsj} (T_{sj} - T_g) - \Delta H_{rg} \quad (5)$$

$$\epsilon_{sj} \rho_{sj} C_{psj} \left(\frac{\partial T_{sj}}{\partial t} + \mathbf{v}_{sj} \cdot \nabla T_{sj} \right) = -\nabla \cdot \mathbf{q}_{sj} - \gamma_{gsj} (T_{sj} - T_g) - \Delta H_{rsj} \quad (6)$$

here T is temperature and \mathbf{q} is the conductive heat flux for gas or solid phase. The γ_{gsj} is the gas-solid heat transfer coefficient considering interphase mass transfer. ΔH_r is the heat of reaction for gas or j^{th} solid phase, respectively.

For species equations

$$\frac{\partial}{\partial t}(\epsilon_g \rho_g Y_{g\alpha}) + \nabla \cdot (\epsilon_g \rho_g Y_{g\alpha} \mathbf{v}_g) = \nabla \cdot D_{g\alpha} \nabla Y_{g\alpha} + R_{g\alpha} \quad (7)$$

$$\frac{\partial}{\partial t}(\epsilon_{sj} \rho_{sj} Y_{sj\beta}) + \nabla \cdot (\epsilon_{sj} \rho_{sj} Y_{sj\beta} \mathbf{v}_{sj}) = \nabla \cdot D_{sj\beta} \nabla Y_{sj\beta} + R_{sj\beta} \quad (8)$$

here Y is the mass fraction and D is diffusion coefficient for chemical species in gas or solid phases. The details of the computational theory and techniques used above governing equations can be found in MFIX documentation theory guide (Syamlal et al. 1993).

Computational Procedure

Figure1 shows the computational domain used in the present study. The nitrogen is issued into the bottom of the reactor uniformly to fluidize the hot sand bed for fast pyrolysis and woody biomass is supplied to the bed at the side of the reactor. Then the product gases and nitrogen

are discharged through reactor outlet located at the top of the reactor. The geometry of bubbling fluidised bed reactor and calculation conditions used in the present study are shown in Table 1. The geometry and calculation conditions are same as Hulme et al. (2005) for the cold flow without reaction. The gas phase consists of three gas species such as nitrogen, tar and non-condensable gas and solid phases are wood, char and sand. In this calculation, voidage of minimum fluidization (ϵ_{mf}) is set as 0.42 and the coefficient of restitution and the angle of internal friction are given as 0.9 and 30° , respectively. For the solid particles, the diameters are set as $200\mu\text{m}$ for sand and $400\mu\text{m}$ for other materials and in this case particles are classified into Geldart B particle (Kunii and Levenspiel 1991). In particular, Syamlal and O'Brien's drag model (1988) for the momentum transfer between solid and fluid is applied in the present study.

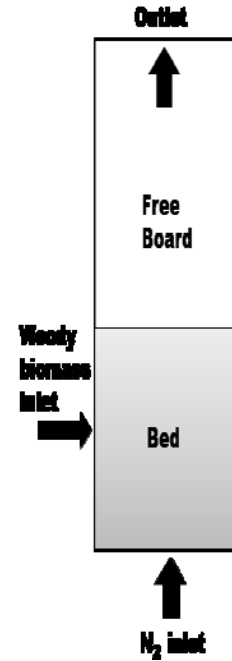


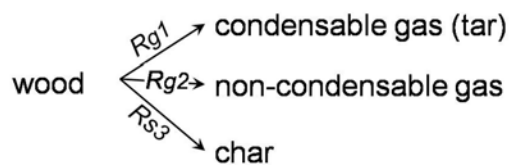
Figure1: Computational domain.

For the temporal discretization, the first-order implicit Euler scheme is used and for spatial one Superbee scheme is adopted with deferred correction method. The time step is changed and adjusted during calculation for reducing total computational time. For pyrolysis reaction calculation, two-stage, semi-global reaction kinetics (Papadakis 2009a, Chan et al. 1985, Blasi 1993, Blasi 1996, Liden et al. 1988) is adopted and Arrhenius type reaction model is applied as $K_i = A_i \exp(-E_i/R_u T)$, here A_i and E_i are pre-exponential factor and activation energy for each species, respectively. The R_u is universal gas constant and their values can be found in Table 1. Hence, for the primary reaction, biomass is decomposed into tar, non-condensable gas and char and for the secondary reaction the produced tar from primary reaction is further decomposed into char and non-condensable gas as in Figure 2.

Computational domain (2- dimensional)	
Length (L)	10 cm
Height (H)	100 cm
Grid allocation (x,y)	20 x 300
Boundary conditions	
N ₂ inlet	Dirichlet ($V_{inlet}=18.6$ cm/s, $T_{inlet}=753$ K)
Woody biomass inlet	Dirichlet ($V_{inlet}=0.21$ cm/s, $T_{inlet}=300$ K)
Outlet	Neumann
Wall	No-slip, Dirichlet($T_{wall}=753$ K)
Particle density	
Wood	0.65 g/cm ³
Char	1.0 g/cm ³
Sand	2.5 g/cm ³
Activation energy	
E_1	2.69E04 cal/mol
E_2	2.12E04 cal/mol
E_3	2.54E04 cal/mol
E_4	2.58E04 cal/mol
E_5	2.58E04 cal/mol
Pre-exponential factor	
A_1	2.0E08 s ⁻¹
A_2	1.3E08 s ⁻¹
A_3	1.0E07 s ⁻¹
A_4	2.6E06 s ⁻¹
A_5	1.0E06 s ⁻¹

Table1: Calculation conditions.

Primary Reaction



Secondary Reaction

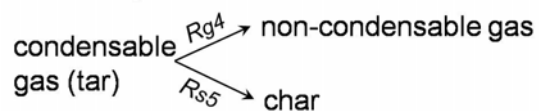


Figure2: Two-step, semi-global reaction mechanism for wood pyrolysis.

RESULTS

Figure3 shows the instantaneous gas and solid phase flow fields by means of their velocity vector map. From Figure3 (a), the local higher regions of the gas velocity magnitude appear inside the gas bubble rising through the sand bed. Around the bubbles, the solid phase flow of sand shows up and down or bursting motions which enhance the mixing between solids and consequent heat transfer from hot sand to wood. This can be confirmed by Figure3(c) and the solid phase of wood follows well with the solid phase of the sand. It is noted that the most vigorous region of solid phase flow is located at the bubble collapsing zone near the instantaneous bed top surface. Figure4 depicts the gas volume fraction (ϵ_g), gas

temperature and the representative primary reaction rate (R_{g1}) and the primary reaction rate involves the production of condensable gas from woody biomass. Here, the other primary reaction rates (R_{g2} , R_{s3}) are omitted for simplicity because they show the very similar pattern like R_{g1} except for their magnitudes. In Figure4 (a), higher gas volume fraction illustrates the bubble region and from the bottom of the bed small bubbles are generated. Then the small bubble is rising and lumps together making bigger bubbles. Finally, the bubble approaches the top of the bed and then collapses resulting in the gas flow downstream the reactor. Comparing the Figure3 (a), the gas velocity increases as the bubble becomes bigger.

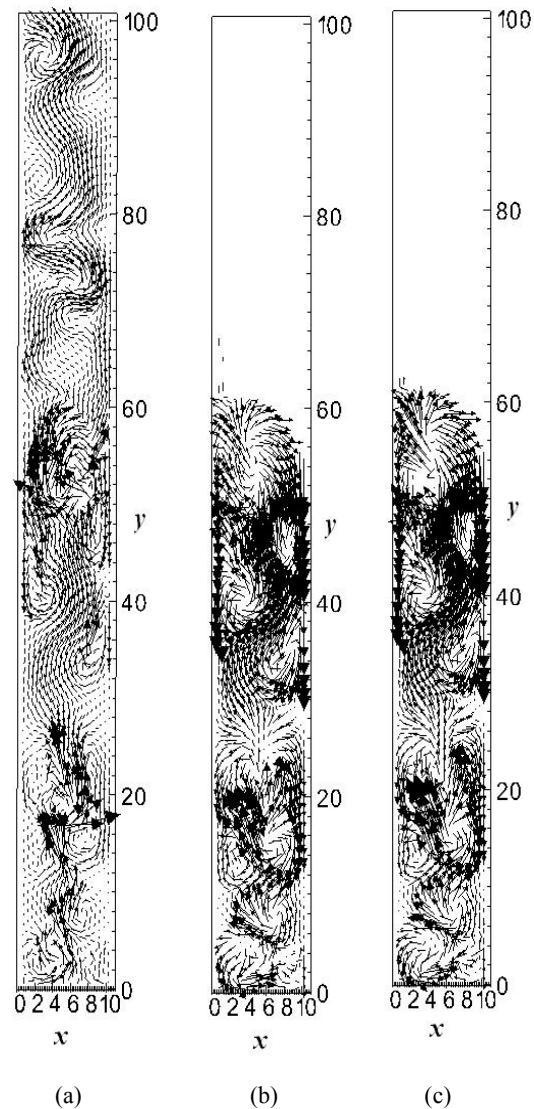


Figure3: The (x, y) velocity vector map; (a) gas phase velocity; (b) solid phase (sand) velocity; (c) solid phase (wood) velocity.

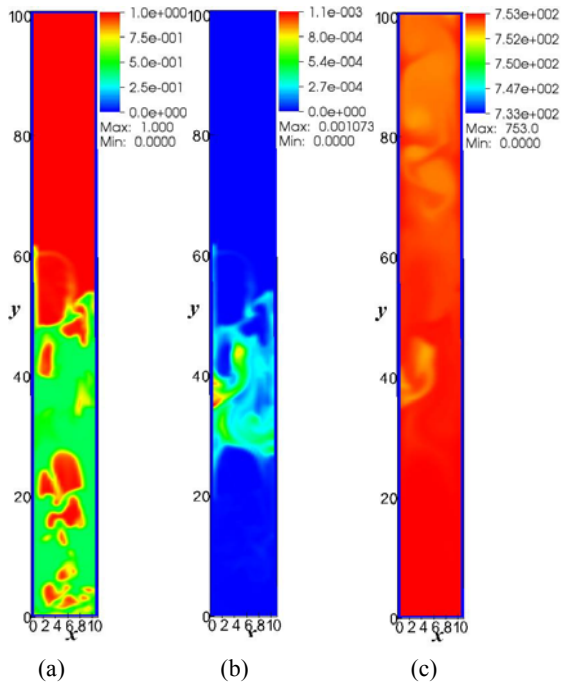


Figure4: The contours of gas volume fraction, primary reaction rate and gas temperature; (a) gas volume fraction (ϵ_g); (b) reaction rate (R_{g1}); (c) gas temperature.

From Figure4 (b), the primary reaction for condensable gas production intensively occurs at woody biomass inlet region and at the region where strong upward solid phase flow exists between bubbles as illustrated in Figure3 (b). Hence, in Figure4 (c), the gas temperature is decreased where the strong primary reaction occurs because the primary reaction of woody biomass is endothermic.

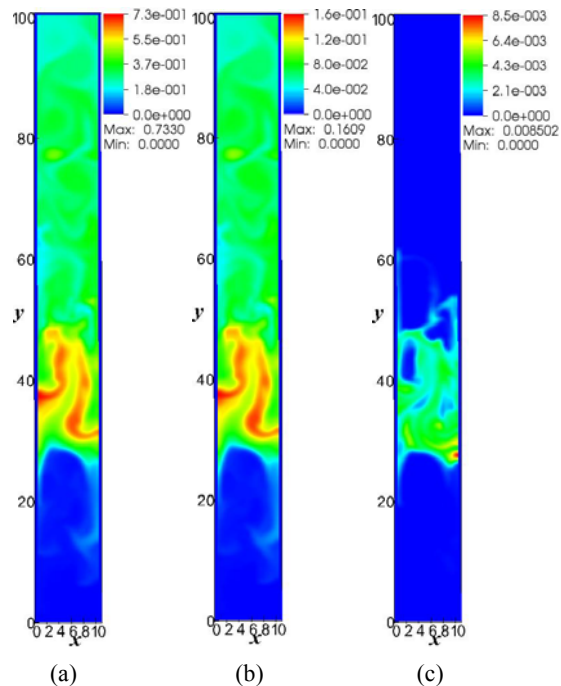


Figure5: The contours of products from the primary reaction; (a) mass fraction of condensable gas; (b) mass fraction of non-condensable gas; (c) density of char.

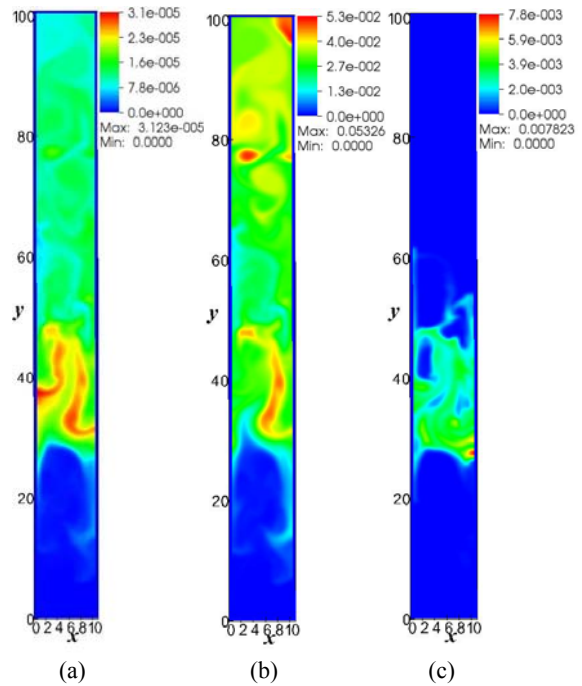
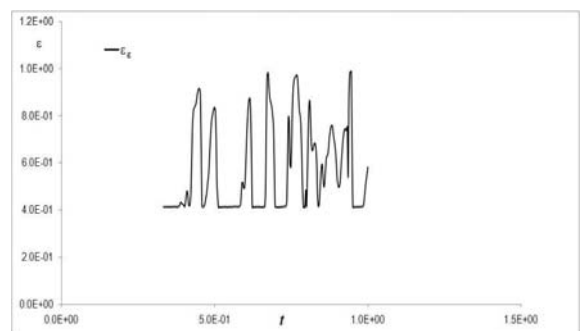
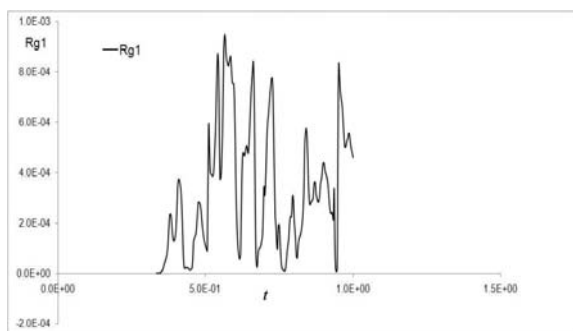


Figure6: The contours of secondary reaction rate and products from the secondary reaction; (a) reaction rate (R_{g4}); (b) mass fraction of non-condensable gas; (c) density of char.

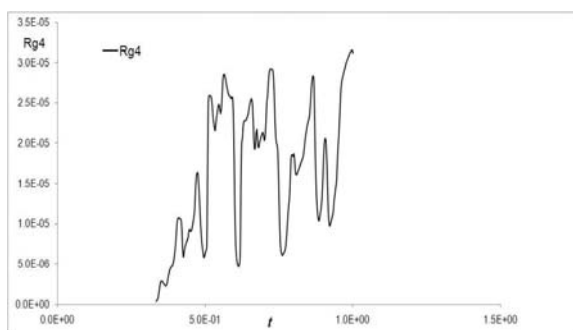
In particular, inside the bubble, the reaction is weaker than the region of solid phase. This can be explained that the wood particles to be decomposed are mainly located at outside the bubble. Figure5 shows the products from the primary reaction, i.e. condensable gas, non-condensable gas and char. The gas is represented by its mass fraction and for solid the effective density by density times volume fraction. The higher region of condensable gas mass fraction is located in the higher primary reaction region of Figure4 (b) and higher gas volume fraction region near the higher primary reaction region, where larger secondary reaction appears as will be discussed in the followings. The contour of non-condensable gas is very similar to condensable gas but the magnitude is decreased as 80% for their maximum values. The char is produced according to the primary reaction (R_{s3}) but it is confined to the solid phase flow. Figure6 shows the secondary reaction rate (R_{g4}) for production of non-condensable gas from the condensable gas generated by primary reaction and the products from the secondary reaction. The non-condensable gas is represented by its mass fraction and char by density times its volume fraction.



(a)



(b)



(c)

Figure7: The distribution of gas volume fraction and reaction rates for a time interval; (a) gas volume fraction (ϵ_g); (b) reaction rate (R_{g1}); (c) reaction rate (R_{g4}).

Also, the other secondary reaction rate (R_{s5}) is omitted for simplicity. In Figure6 (a), the secondary reaction occurs at the region where intensive primary reaction is generated as well as inside the gas bubbles as discussed before. The reaction also arises far downstream of the gas flow outside the sand bed, because the condensable gas produced from the primary reaction is convected toward inside and outside the bed. Then the secondary reaction may be generated where the condensable gas exists. It is noted that the mass fraction for non-condensable gas is decreased as 33% compared with that of the primary reaction at their maximum values but the non-condensable gas is still produced at far downstream from the fluidising bed. Hence, it is better that the condensable gas is extracted from the reactor above the fluidising bed as close as possible from the bed.

To look into the time characteristics of the gas-solid flow and its effect to the reaction rate, Figure7 shows the distribution of the gas volume fraction and reaction rates for a time interval at the sampling position of $x=1.25\text{cm}$, $y=39.5\text{cm}$ inside the fluidising bed. Figure7 (a) illustrates bubble rising with the passage of the time and within the time interval several bubbles are passed through the sampling point. The peak of the primary reaction rate coincides with the lowest gas volume fraction which matches to the solid phase region. Whereas the peak position of the secondary reaction rate occurs both in the the lowest gas volume fraction and high gas volume fraction region. So, it is noted that the population of the secondary tar cracking reaction is more frequent than that of the primary reaction but the magnitude is much lower in the secondary reaction.

CONCLUSION

In the present study, the numerical simulation for the fast pyrolysis of the bubbling fluidised bed reactor is carried out to investigate the effect of gas-solid flow field on the fast pyrolysis reaction. To simulate the fast pyrolysis of woody biomass, two-step, semi-global chemical kinetics is applied including the secondary tar cracking reaction. From the results, the peak primary reaction occurs in the vigorous solid phase flow between bubbles near the woody biomass inlet and products spread over the fluidising bed by the intensive solid phase flow according to the related bubble motions. However, the secondary tar cracking reaction is processed where the mass fraction of condensable gas is large and above the fluidising bed at far downstream of the solid phase flow the tar cracking mechanism still works. Hence, it is better that the condensable gas is extracted from the reactor above the fluidising bed as close as possible from the bed. Over the time interval, the same pattern of the reactions is repeated as illustrated before. Especially, the population of the secondary tar cracking reaction is more frequent than that of the primary reaction but the magnitude is much lower in the secondary reaction. From the present study, the flow and reaction fields for the fast pyrolysis of woody biomass are fully scrutinized and the CFD technique will be applied to optimal design of the reactor for its scale-up having lower tar cracking reaction.

REFERENCES

- BRAMMER, J.G., LAUER, M., BRIDGWATER, A.V., (2006), "Opportunities for biomass-derived "bio-oil" in European heat and power markets", *Energy Policy*, **34**, 2871-2880.
- DONG, L., LIU, H., RIFFAT, S., (2006), "Development of small-scale and micro-scale biomass-fuelled CHP systems – a literature review", *Applied Thermal Engineering*, **29**, 2119-2126.
- WU, C., YIN, X., MA, L., ZHOU, Z., CHEN, H., (2009), "Operation characteristics of a 1.2-MW biomass gasification and power generation plant", *Biotechnology Advances*, **27**, 588-592.
- DAHL, O., NURMESNIEMI, H., POYKIO, R., WATKINS, G., (2009), "Comparison of the characteristics of bottom ash and fly ash from a medium-size (32 MW) municipal district heating plant incinerating forest residues and peat in a fluidized-bed boiler", *Fuel Processing Technology*, **90**, 871-878.
- PARK, H., PARK, Y., KIM, J., (2008), "Influence of reaction conditions and the char separation system on the production of bio-oil from radiate pine sawdust by fast pyrolysis", *Fuel Processing Technology*, **89**, 797-802.
- ZHENG, J., (2008), "Pyrolysis oil from fast pyrolysis of maize stalk", *J. Anal. Appl. pyrolysis*, **83**, 205-212.
- VELDEN, M., BAEYENS, J., BOUKIS, I., (2008), "Modeling CFB biomass pyrolysis reactors", *Biomass and Bioenergy*, **32**, 128-139.
- SAASTAMOINEN, J.J., (2006), "Simplified model for calculation of devolatilization in fluidized beds", *Fuel*, **85**, 2388-2395.
- PAPADIKIS, K., GU, S., BRIDGWATER, A.V., (2009a), "CFD modelling of the fast pyrolysis of biomass in fluidised bed reactors. Part B heat, momentum and mass transport in bubbling fluidised bed", *Chemical Engineering Science*, **64**, 1036-1045.

PAPADIKIS, K., GU, S., BRIDGWATER, A.V., GERHAUSER, H., (2009b), "Application of CFD to model fast pyrolysis of biomass", *Fuel Processing Technology*, **90**, 504-512.

SYAMLAL, M., ROGERS, W., O'BRIEN, T.J., (1993), "MFIIX documentation theory guide", Technical Note, DOE/METC-94/1004, NTIS/DE94000087, U.S. Department of Energy, Office of Fossil Energy, Morgantown Energy Technology Center Morgantown, WV, National Technical Information Service, Springfield, VA .

WACHEM, B.G. M., SCHOUTEN, J.C., BLEEK, C.M., KRISHNA, R., SINCLAIR, J. L., (2001), "Comparative analysis of CFD models of dense gas-solid systems", *AIChE Journal*, **47**, 1035-1051.

HULME, I., CLAVELLE, E., VAN DE LEE, L., KANTZAS, A., (2005), "CFD modeling and validation of bubble properties for a bubbling fluidized bed", *Ind. Eng. Chem. Res.*, **44**, 4254-4266.

KUNII, D., LEVENSPIEL, O., (1991), "Fluidization Engineering", second edition, Butterworth-Heinemann.

SYAMLAL, M, O'BRIEN, T. J., (1988), "Simulation of Granular Layer Inversion in Liquid Fluidized Beds", *Int. J. Multiphase Flow*, **14**, 473-481.

CHAN, W.R., KELBON, M., KRIEGER, B.B., (1985), "Modeling and experimental verification of pyrolysis and chemical processes during pyrolysis of large biomass particle", *Fuel*, **64**, 1505-1513.

BLASI, C.D., (1993), "Analysis of convection and secondary reaction effects within porous solid fuels undergoing pyrolysis", *Combustion Science Technology*, **90**, 315-339.

BLASI, C.B., (1996), "Heat, momentum and mass transport through a shrinking biomass particle exposed to thermal radiation", *Chemical Engineering Science*, **51**, 1121-1132.

LIDEN, A.G., BERRUTI, F., SCOTT, D.S., (1988), "A kinetic model for the production of liquids from the flash pyrolysis of biomass", *Chemical Engineering Communications*, **65**, 207-221.